Biosensors and Bioelectronics 64 (2015) 611–617

Contents lists available at ScienceDirect

Biosensors and Bioelectronics

journal homepage: www.elsevier.com/locate/bios

Construction of photoelectrochemical thrombin aptasensor via assembling multilayer of graphene–CdS nanocomposites

Li Shangguan [a], Wei Zhu [b], Yanchun Xue [b], Songqin Liu [a,c,*]

[a] Jiangsu Province Hi-Tech Key Laboratory for Bio-medical Research, School of Chemistry and Chemical Engineering, Southeast University, Nanjing 210096, PR China
[b] Jingjiang People's Hospital, PR China
[c] Suzhou Research Institute of Southeast University, PR China

ARTICLE INFO

Article history:
Received 5 July 2014
Received in revised form
25 September 2014
Accepted 25 September 2014
Available online 28 September 2014

Keywords:
Photoelectrochemical
Thrombin
Aptamer
Graphene–CdS
Hexaammineruthenium(III) chloride

ABSTRACT

A photoelectrochemical (PEC) aptasensor for highly sensitive and specific detection of thrombin was developed by using graphene–CdS nanocomposites multilayer as photoactive species and electroactive mediator hexaammineruthenium(III) chloride ($Ru(NH_3)_6^{3+}$) as signal enhancer. Graphene–CdS nanocomposites (G–CdS) were synthesized by one-pot reduction of oxide graphene and $CdCl_2$ with thioacetamide. The photoactive multilayer was prepared by alternative assembly of the negatively charged 3-mercaptopropionic acid modified graphene–CdS nanocomposites (MPA-G–CdS) and the positively charged polyethylenimine (PEI) on ITO electrode. This layer-by-layer assembly method enhanced the stability and homogeneity of the photocurrent readout of G–CdS. Thrombin aptamer was covalently bound to the multilayer by using glutaraldehyde as cross-linking. Electroactive mediator $Ru(NH_3)_6^{3+}$ could interact with the DNA phosphate backbone and thus facilitated the electron transfer between G–CdS multilayer and electrode and enhanced the photocurrent. Hybridizing of a long complementary DNA with thrombin aptamer could increase the adsorption amount of $Ru(NH_3)_6^{3+}$, which in turn boosted the signal readout. In the presence of target thrombin, the affinity interaction between thrombin and its aptamer resulted in the long complementary DNA releasing from the G–CdS multilayer and decreasing of photocurrent signal. On the basis of G–CdS multilayer as the photoactive species, $Ru(NH_3)_6^{3+}$ as an electroactive mediator, and aptamer as a recognition module, a high sensitive PEC aptasensor for thrombin detection was proposed. The thrombin aptasensor displayed a linear range from 2.0 pM to 600.0 pM and a detection limit of 1.0 pM. The present strategy provided a promising ideology for the future development of PEC biosensor.

1. Introduction

Recently, photoelectrochemical (PEC) biosensing platform has attracted considerable attention from many fields, such as clinical diagnosis, biomedical research, environmental analysis, and food quality control. PEC method has the advantages of simple, rapid and high sensitivity applied in analysis of life science. Some PEC sensors have been developed for sensitive detection of immune molecules (Li et al., 2013; Zhao et al., 2012a, 2012b; Hu et al., 2013), DNA damage (Zhao et al., 2012c; Yin et al., 2014), cancer cells (Zhao et al., 2012d; Qian et al., 2010), pesticide (Xiao et al., 2012) and some small molecules (Tu et al., 2011; Wang et al., 2010; Shi et al., 2011). The general PEC biosensing mechanism is that the specific recognition reactions are converted into the corresponding photocurrent signals change. These conversions usually need the help of photoactive species. Up to now, semiconductor nanoparticles such as CdS (Wang et al., 2009a, 2009b; Sun et al., 2014; Tian et al., 2012), TiO_2 (Guo et al., 2014; An et al., 2010; Wang et al., 2009a; Huang et al., 2013; Zhao et al., 2013; Li et al., 2012), CdSe (Zhang et al., 2011a, 2011b; Tanne et al., 2011; Bas and Boyacı, 2009), ZnO (Li et al., 2014a; Shen et al., 2011), SnO_2 (Wang et al., 2013), and CdTe (Zeng et al., 2013), metal complex (such as phthalocyanine (Li et al., 2013), rutheniumbipyridine derivatives (Liang et al., 2006; Yao et al., 2013; Zhang et al., 2010)), and conjugated polymers (Li et al., 2011) have been employed as photoactive species in these conversions. On the other hand, graphene, a two-dimensional (2-D) nanomaterial consisting of sp^2-hybridized carbon atoms and forms a one-atom thick honeycomb lattice, also being considered as a promising candidate for electron-acceptor and electron-transfer material due to its excellent optical and electrical properties (Lin et al., 2010). The

* Corresponding author at: Jiangsu Province Hi-Tech Key Laboratory for Bio-medical Research, School of Chemistry and Chemical Engineering, Southeast University, Nanjing 210096, PR China. Fax: +86 25 52090618.
E-mail address: liusq@seu.edu.cn (S. Liu).

http://dx.doi.org/10.1016/j.bios.2014.09.072
0956-5663/

nanocomposites of graphene-semiconductor nanocomposites were skillfully constructed and used as the photoactive species for biosensing (Li et al., 2013; Sun et al., 2014). For example, Zhu and co-workers prepared graphene–CdS nanocomposites for the fabrication of photoelectrochemical cytosensor (Zhao et al., 2012d). The as-prepared nanocomposites films inherited the excellent electron transport properties of graphene, facilitated the spatial separation of the charge carriers and enhanced photocurrent intensity. The resulting cytosensor displayed a good photoelectronic effect and cell-capture ability with a wide linear range and low detection limit for Hela cells.

Human thrombin is a serine protease and does not find in healthy blood (Li et al., 2010). Over-expression or activity imbalance of thrombin is associated with many diseases such as thrombosis, inflammation, atherosclerosis, and hemophilia (Li et al., 2014b). Therefore, accurate detection of thrombin concentration is valuable for disease diagnosis and drug discovery. Some methods had been applied for thrombin determination. For example, Crooks et al. developed an electrochemical device for detection of DNA and thrombin, using methylene blue (MB) as the electroactive reporter (Cunningham et al., 2014). Xiao et al. reported an electrochemical thrombin aptasensor by covalent binding thrombin aptamer onto graphene modified electrode (Wang et al., 2012a). Xiang et al. reported an electrochemiluminescence sensing strategy by $Ru(phen)_3^{2+}$ using $Ru(phen)_3^{2+}$ as the signal probe coupling with nuclease-assisted recycling amplification for detection of thrombin (Yang et al., 2014). Li et al. prepared a silver nanoparticles–dyes–gold ultrathin film for fluorescence thrombin determination (Cao et al., 2014). The fluorescence was generated from the directional surface Plasmon coupled between nanoparticles and dyes. A PEC biosensor fabricated by using carboxyl-functionalized graphene and CdSe nanoparticles was also proposed for sensitive detection of thrombin (Zhang et al., 2012). The dual-quenched effect based on the electron transfer of a bipyridinium relay and energy transfer of AuNPs was investigated.

This work was also motivated by very promising applications of the nanostructured photoactive materials for PEC biosensing. As a proof of the concept, hexaammineruthenium(III) chloride ($Ru(NH_3)_6^{3+}$) was used as an electroactive mediator, while MPA modified G–CdS nanocomposites was used as photoactive species, to fabricate a PEC bioanalytical protocol with model analyte of thrombin. The detailed fabrication process of the PEC aptasensor was described in Scheme 1. The stable and uniform photoactive multifilms were fabricated by the layer-by-layer assembly method based on the alternating adsorption of oppositely charged species in solution. MPA modified G–CdS nanocomposites was beneficial for increasing the stability and availability of the photoactive multifilms. Thrombin aptamer was immobilized covalently on the ITO electrode surface by GA cross-linking. On the basis of the MPA-G–CdS nanocomposites as the photoactive species, $Ru(NH_3)_6^{3+}$ as an electroactive mediator, and aptamer as a recognition module, a high sensitive PEC aptasensor for thrombin detection was proposed.

2. Experimental section

2.1. Materials and reagents

Bovine serum albumin (BSA) was obtained from Sunshine Biotechnology Co. Ltd. (Nanjing, China). Poly(sodium-*p*-styrenesulfonate) (PSS) and 3-mercaptopropionic acid (MPA) were the products of J&K Scientific Ltd. (Beijing, China). Hemoglobin from bovine blood (Hb), lysozyme, tris(hydroxymethyl)aminomethane (Tris), ascorbic acid (AA) and glutaraldehyde (GA, 25% aqueous solution) were purchased from Sinopharm Chemical Reagent Co. Ltd. (Shanghai, China). Polyethyleneimine (PEI) and $CdCl_2$ were obtained from Aladdin Industrial Co. (Shanghai, China). Thioacetamide (TAA) was received from Shanghai Chemical Reagent Co. Ltd. (Shanghai, China). Hexaammineruthenium (III) chloride ($Ru(NH_3)_6^{3+}$), acetylcholine esterase (AchE), glucose oxidase (GOD) and human α-thrombin (thrombin, 37.4 kDa, 2949 NIH units/mg protein, p*I*=6.35–7.6) were purchased from Sigma-Aldrich (Shanghai, China). Thrombin aptamer (5′-NH_2-$(CH_2)_6$-TTTTTGGTTGGTGTGGTTGG-3′) and the long complementary DNA (5′-NH_2-$(CH_2)_6$-TTTTTTTTTTTTTTTTTTTTCCAACCACACCAACC-3′) were synthesized by Shanghai Sangon Biotech Co. Ltd. (Shanghai, China). 0.1 M phosphate buffer (PBS, pH 7.4) was used for preparation of aptamer solution, while 0.1 M pH 7.4 Tris–HCl buffer containing 1.0 M NaCl was used for preparation of complementary DNA solution. Oxide graphene (GO) was synthesized according to previous literatures (Tian et al., 2012). Serum samples were obtained from Southeast University Hospital. All other reagents were of analytical grade and used as received. Deionized water from Thermo Scientific Nanopure Water Purifier (18.2 MΩ cm) was used throughout the experiments.

2.2. Apparatus

Scanning electron microscopy (SEM, Ultra Plus, Zeiss, Germany) and transmission electron microscopy (TEM, JEM-2100, Japan) were used to examine the morphology of nanocomposites. The photocurrent was measured on a CHI 832b electrochemical workstation (Shanghai, China) with a three-electrode system, whereas the ITO electrode (0.5 cm × 5.0 cm) was used as the working electrode, a platinum wire was used as the counter electrode, and a saturated Ag/AgCl electrode was used as the reference electrode. A 150 W Xe lamp (Zolix instrument, Beijing, China) was used as an irradiation source. The light intensity of the work electrode surface about 16 mW cm^{-2} estimated with a radiometer (HD2302 Light Meter, Delta OHM). All of the photocurrent measurements were carried out in PBS (0.1 M, pH 7.4) containing 0.1 M AA, which was fresh preparation. The applied potential was +0.2 V (versus Ag/AgCl). Electrochemical impedance spectroscopy (EIS) was carried out at open circuit potential with the Versa STAT 3 (Riceton Applied Research, UK) in 0.1 M KCl solution containing 5.0 mM $K_3Fe(CN)_6$/$K_4Fe(CN)_6$ (1:1) as redox probe from 0.01 Hz to 25 kHz with a signal amplitude of 10 mV.

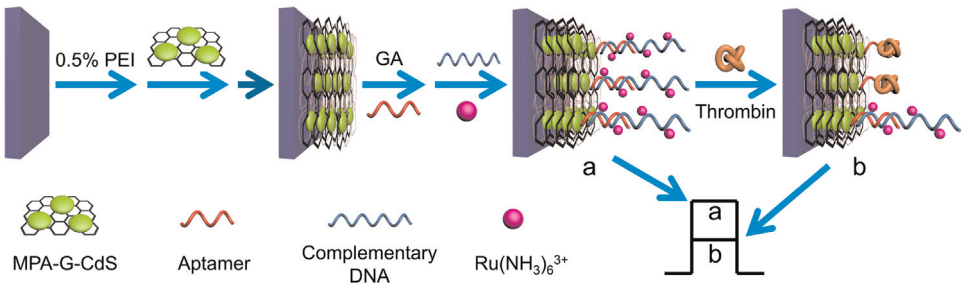

Scheme 1. Schematic diagram for the preparation of thrombin aptasensor.

2.3. Preparation of MPA-G–CdS nanocomposites

The preparation of MPA-G–CdS nanocomposites was according to previous report with a little modification (Li et al., 2013). Briefly, 50 μL 2.0 mg mL^{-1} GO was dispersed in 30 mL 0.5% PSS solution and ultra-sonicated for 30 min. Then 10 mL 11.4 mg mL^{-1} $CdCl_2$ solution in water was added under vigorous stirring for another 30 min. Finally, 10 mL 10 mg mL^{-1} TAA solution in water was added and kept at 80 °C for 2 h under stirring. The resulting G–CdS nanocomposites were separated by centrifugation at 9000 rpm for 10 min, washed with deionized water for three times, and then dispersed in 0.1 M MPA solution under stirring for 30 min, followed purification by ultrasonication and centrifugation. The resulting MPA-G–CdS nanocomposites were dispersed in deionized water to final volume of 8 mL for following use. The procedure for preparing MPA-CdS nanoparticles was analogous with the aforementioned without the addition of GO.

2.4. Preparation of PEC aptasensor

The PEC aptasensor was fabricated by layer-by-layer (LBL) assembly photoactive species based on the alternating adsorption of oppositely charged species (Wang et al., 2009a). The ITO slice was ultra-sonicated for 15 min in acetone, ethanol and deionized water, respectively. Then, it was treated with 1.0 M NaOH for 10 min, carefully washed with deionized water and dried at 120 °C. The photoactive multifilms ($(PEI/MPA\text{-}G\text{–}CdS)_n$) on ITO slice were grown by alternately dipping of the cleaned ITO slice into a solution of 0.5% PEI and the as-obtained MPA-G–CdS nanocomposites suspension for each 15 min. The film was washed with deionized water after each dipping step and dried under N_2 atmosphere. This process was repeated to obtain a desired layer number. Conjugation of aptamers onto photoactive multifilms was achieved by using GA cross-linking. 10 μL 2.5% GA solution was casted on multifilms with outside layer of PEI and allowed to react for 1 h at room temperature. After washing with deionized water, 20 μL 10 μM thrombin aptamer solution was dropped on ITO surface and allowed to react at 4 °C for 12 h. The unbound aldehyde groups could be inactivation by immersing of the resultant film in 0.1 M pH 7.4 Tris–HCl buffer for 2 h (Deng et al., 2013). Then, 20 μL 10 μM long complementary DNA in Tris–HCl buffer was casted on the resulting ITO slice. The hybridization reaction occurred at 37 °C for 2 h. Finally, 20 μL 0.1 mM $Ru(NH_3)_6^{3+}$ was dropped on the resulting ITO slice and reacted for 30 min. This step allowed $Ru(NH_3)_6^{3+}$ to be absorbed on the DNA phosphate backbone. Between each step, the ITO slice was washed thoroughly with deionized water to remove the non-significant interaction molecules. The same process was for the experiment without absorption of $Ru(NH_3)_6^{3+}$. The whole procedure for preparation of aptasensor was illustrated in Scheme 1.

For the PEC analysis, 20 μL thrombin solutions with different concentrations in PBS or in diluted ten times serum sample were casted on the aptasensor and incubated at room temperature for 30 min. After washing with deionized water thoroughly, the aptasensor interacted with $Ru(NH_3)_6^{3+}$ liking the aforementioned process and measured the photocurrent signals in AA solution.

3. Results and discussion

3.1. Construction of photoelectrochemical platform

The as-synthesized MPA-G–CdS was demonstrated by TEM and SEM. After reducing with TAA, the CdS nanoparticles were uniformly grown on both sides of graphene sheets with about 50 nm diameter (Fig. 1). SEM image of G–CdS nanocomposites indicated that graphene sheet was densely decorated with CdS particles (Fig. S-2). High-resolution TEM image showed the obvious lattice fringe, which was assigned to the (100) plane of hexagonal CdS (Fig. S-3b) (Li et al., 2013), while the graphene still kept a sheet structure. Besides, some unattached CdS particles composing dozens of small primary nanocrystals were uniform distribution (Fig. S-3a).

The G–CdS was further treated by MPA to enhance the negative charge of the G–CdS nanocomposites. The zeta potential of G–CdS nanocomposites measured by the zeta potential analysis (Zatasizer nano, Malvern) was −15.6 mV, similar to the other reported work (Li et al., 2013). After modification with MPA, the zeta potential for MPA-G–CdS nanocomposites was increased to −48.8 mV (Fig. S-4), which was more negative than PSS enwrapped G–CdS nanocomposites, confirming the successful modification of G–CdS by MPA.

PEI was one of cationic macromolecules with many amine groups. The positive charged PEI was easy to be adsorbed onto the pretreated negative charged hydroxylated ITO surface, which in turn led to follow alternate assembly between PEI and MPA-G–CdS nanocomposites. To investigate the effect of MPA and graphene on the construction of PEC platform, the photocurrent signals of the ITO slice modified four layers with PEI/G–CdS, PEI/MPA-CdS and PEI/MPA-G–CdS were measured, respectively. As shown in Fig. S-5, the $(PEI/MPA\text{-}G\text{–}CdS)_4$ modified ITO electrode displayed a largest photocurrent of 7.9 μA (curve c). $(PEI/MPA\text{-}CdS)_4$ modified ITO displayed a photocurrent of 4.0 μA (curve b), which was larger than that of 2.2 μA for $(PEI/G\text{–}CdS)_4$ modified ITO (curve a), but was near twice smaller than that of $(PEI/MPA\text{-}G\text{–}CdS)_4$ modified ITO electrode. Thus, both MPA and graphene enhanced the assembly efficiency of photoactive multifilms, and improved the quantity of photoactive species on the electrode surface at the same condition. Graphene was a promising candidate for electron-acceptor and electron-transfer material, which could effective transfer photoelectrons from the conduction band (CB) of CdS to the ITO electrode and led to increase the photocurrent signal readout (Li et al., 2013).

Meanwhile, the photocurrent of $(PEI/MPA\text{-}G\text{–}CdS)_n$ modified ITO slice depended on the layer numbers of PEI/MPA-G–CdS. As shown in Fig. S-6, the photocurrent of $(PEI/MPA\text{-}G\text{–}CdS)_n$ modified ITO slice was increased with the layer numbers from 0 to 4, while negligible photocurrent could be observed from the bare ITO slice, indicating the increasing amount of adsorbed MPA-G–CdS nanocomposites on ITO slice during the LBL assembly procedure. Further increasing the layer numbers, e.g., $(PEI/MPA\text{-}G\text{–}CdS)_5$ and $(PEI/MPA\text{-}G\text{–}CdS)_6$, led to the photocurrent increase slowly comparing with the front films. This might be explained that too much photoactive species on LBL films influenced the diffusion between the electron-donor and the surface of MPA-G–CdS nanocomposites

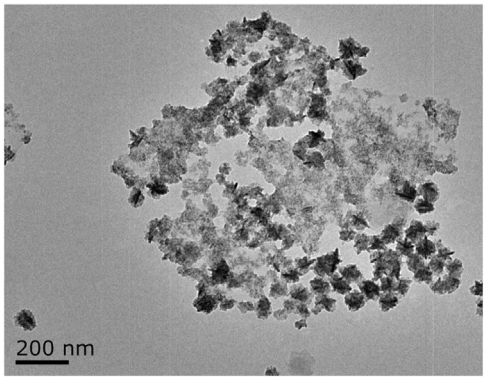

Fig. 1. TEM image of the MPA-G–CdS nanocomposites.

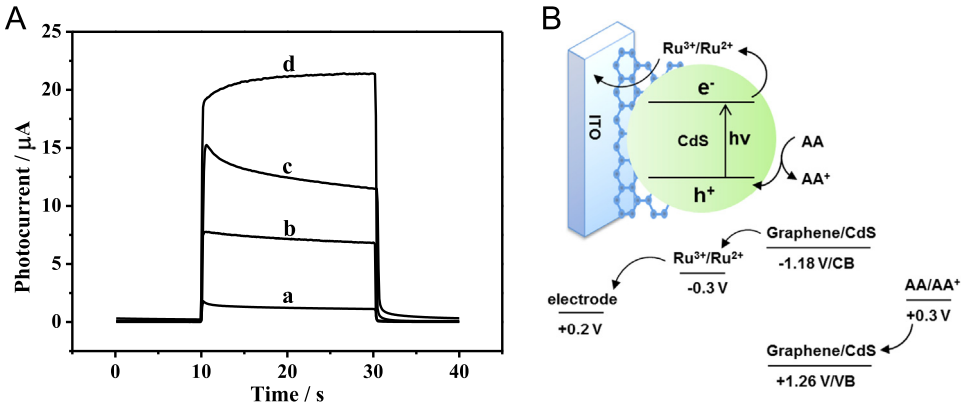

Fig. 2. (A) The corresponding photoelectrochemical responses of the ITO/(PEI/MPA-G–CdS)$_4$ electrode in (a) 0.1 M PBS, (b) 0.1 M PBS containing 0.1 M AA. (c) The ITO/(PEI/MPA-G–CdS)$_4$ electrode treated with $Ru(NH_3)_6^{3+}$ and measured in 0.1 M PBS and (d) was (c) measured in 0.1 M PBS containing 0.1 M AA. The applied potential was +0.2 V. (B) PEC generation mechanism at the ITO/(PEI/MPA-G–CdS)$_4$ electrode with an effective electron donor system.

(Peng et al., 2012). Considering the time and labor, (PEI/MPA-G–CdS)$_4$ was chosen in the later test.

3.2. *Influence of* $Ru(NH_3)_6^{3+}$ *on photocurrent Responses*

$Ru(NH_3)_6^{3+}$ was an effective sensitizer for enhancement of the photocurrent readout of (PEI/MPA-G–CdS)$_n$ nanocomposites. As shown in Fig. 2A, ITO/(PEI/MPA-G–CdS)$_4$ had about 2.0 μA photocurrent in 0.1 M PBS under irradiating with visible light (curve a). The observed photocurrent came from the oxidization of water or hydroxide ions to hydroxyl radicals by electron–hole of CdS produced by light irradiation (Ipe et al., 2005). In the presence of 0.1 M AA as the sacrificial electron-donor, the photocurrent of ITO/(PEI/MPA-G–CdS)$_4$ electrode increased near 4 times (curve b), which was good agreement with previous reports in PEC analysis (Zhao et al., 2012a, 2012d; Wang et al., 2009a; Sun et al., 2014). After the ITO/(PEI/MPA-G–CdS)$_4$ electrode was incubated in 0.1 mM $Ru(NH_3)_6^{3+}$ for 30 min, the photocurrent of the resulting electrode increased remarkably to 15.0 μA in 0.1 M PBS without AA and 22.0 μA in 0.1 M PBS containing 0.1 M AA, respectively (curves c and d). Therefore, both AA and $Ru(NH_3)_6^{3+}$ accelerated the photoelectron-transfer and led to increase the photocurrent. In addition, the photocurrent had an obvious decay without AA (curve c) during the light radiation comparing with that in the presence of electron-donor AA in solution (curve d). This is due to the diffusion of electron-donor slower than the transmission of photoelectrons.

Fig. 2B shows the mechanism of photocurrent generation by MPA-G–CdS nanoparticles under irradiation. Under the irradiation, the CdS QDs were excited to generate electron–hole pair (excitations) (Qian et al., 2010; Huang et al., 2013), which then underwent the electron transfer process between the CB and VB (Gill et al., 2005). When the electrode potential was at the positively applied bias, the CB electrons was transferred to the electrode yield the photocurrent, while AA supplied the electrons of VB holes, completed the photocurrent generation cycle. Graphene enhanced the electron-transfer and impeded the electron recombination. In the presence of $Ru(NH_3)_6^{3+}$ in the solution, electrons from the CB of QDs could reduce $Ru(NH_3)_6^{3+}$ to $Ru(NH_3)_6^{2+}$. The produced $Ru(NH_3)_6^{2+}$ was oxidized by electrode and resulted in the enhancement of photocurrent. Therefore, the electroactive mediator $Ru(NH_3)_6^{3+}$ on CdS nanoparticles was easier to get electrons from CB of CdS and improved the photo-to-current conversion efficiency.

The influence of the applied potential on the generation of photocurrent was investigated. With increasing of potential from 0 to +0.2 V, the photocurrent signals had a sharp increase (Fig. S-7A). When the applied potential was more than +0.3 V, the photocurrent signals decreased gradually, due to that the electron-donor AA was electrochemical oxidized. Thus, +0.2 V was selected as the applied potential. The stability of the photocurrent readout of the as-prepared PEC system was illustrated. The photocurrent could keep over 99% of its original intensity when the light turned on and off for over 20 cycles with every ten seconds, confirming a good reversibility and stability (Fig. S-7B).

3.3. *Interaction between DNA and* Ru^{3+}

After aptamer coupling and further hybridization with long complementary DNA, the photocurrent signals of resulting both electrodes (ITO/(PEI/MPA-G–CdS)$_4$/aptamer and ITO/(PEI/MPA-G–CdS)$_4$/aptamer–DNA) were decreased slightly (Fig. S-8, regions a–c, white column), confirming the successfully bound of aptamer and long complementary DNA to the ITO electrode. However, when both ITO/(PEI/MPA-G–CdS)$_4$/aptamer and ITO/(PEI/MPA-G–CdS)$_4$/aptamer–DNA immersing in $Ru(NH_3)_6^{3+}$ solution, the $Ru(NH_3)_6^{3+}$ could be adsorbed onto the aptamer or double-stranded DNA modified multilayer through the strong electrostatic interaction between the positively charged $Ru(NH_3)_6^{3+}$ and the negatively charged DNA, resulting in a large photocurrent signals (Fig. S-8, regions a–c, black column). In addition, the photocurrent for ITO/(PEI/MPA-G–CdS)$_4$/aptamer–DNA was much larger than that for ITO/(PEI/MPA-G–CdS)$_4$/aptamer, indicating that the double DNA chain could absorb more $Ru(NH_3)_6^{3+}$. More $Ru(NH_3)_6^{3+}$ on double DNA chain could be demonstrated by using chronocoulometric analysis based on effective electrode area of 0.24 cm^2. It explored that the $Ru(NH_3)_6^{3+}$ densities at ITO/(PEI/MPA-G–CdS)$_4$/aptamer and ITO/(PEI/MPA-G–CdS)$_4$/aptamer–DNA were 1.01×10^{-11} mol cm^{-2} and 1.21×10^{-11} mol cm^{-2}, respectively (Sato and Takenaka, 2012).

Fig. 3 shows the photoelectrochemical characterization of aptasensor fabrication steps. It was hard observation the photocurrent response on the bare ITO electrode (curve a) with the light on and off. Fabricating four layers photoactive films on the electrode surface showed obvious photocurrent of 7.2 μA (curve b). It indicated that the photoactive species had been immobilized on the electrode surface. As the statement aforementioned, in the case of PEI, aptamer and the long complementary DNA interaction with ITO/(PEI/MPA-G–CdS)$_4$ electrode sequent, the photocurrent signals had decreased gradually to 2.7 μA, 1.16 μA and 0.75 μA, respectively (curves c, d and e). After the electrode absorbed $Ru(NH_3)_6^{3+}$, the photocurrent had a great increase to 22.3 μA (curve f). It proved that $Ru(NH_3)_6^{3+}$ being absorbed on DNA chain still was effective for enhancing electron-transfer. After aptasensor

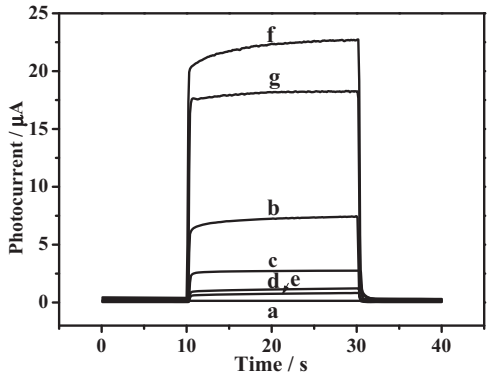

Fig. 3. The corresponding photoelectrochemical responses of bared ITO (a), ITO/(PEI/MPA-G–CdS)$_4$ (b), ITO/(PEI/MPA-G–CdS)$_4$/PEI (c), ITO/(PEI/MPA-G–CdS)$_4$/PEI/aptamer (d), ITO/(PEI/MPA-G–CdS)$_4$/PEI/aptamer–DNA (e), ITO/(PEI/MPA-G–CdS)$_4$/PEI/aptamer–DNA electrodes absorbed $Ru(NH_3)_6^{3+}$ and after interaction with 4.0 pM thrombin (f, g) measured in 0.1 M AA at +0.2 V.

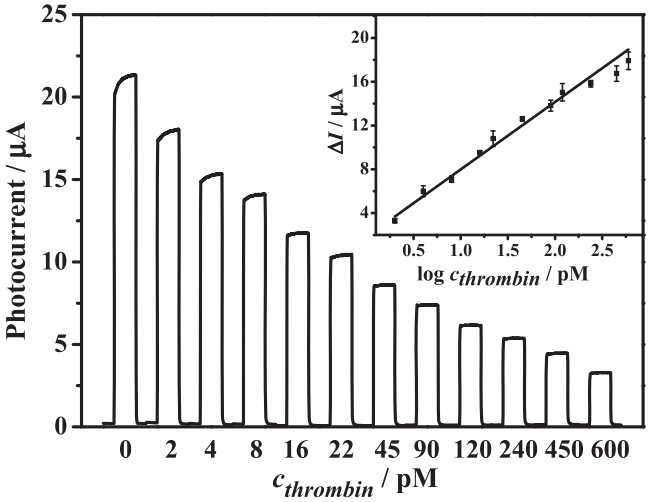

Fig. 4. The photocurrent curves of the PEC aptasensor showed the thrombin concentrations from 0 to 600.0 pM, which measured in 0.1 M AA at +0.2 V. The inset showed the corresponding calibration curve between the photocurrent decrement (ΔI) and the logarithmic value of the thrombin concentration.

interaction with thrombin, the photocurrent signals had obvious reduced (curve g). It explained that thrombin replaced the long complementary DNA, which not only partly hindered the diffusion of the sacrificial electron-donor, but also decreased the amount of $Ru(NH_3)_6^{3+}$ on the electrode surface.

The assembly process of the aptasensor was investigated by electrochemical impedance spectroscopy (Fig. S-9). The bare ITO electrode exhibited a small electron-transfer resistance (R_{et}) of 35 Ω, proved that the treated ITO electrode had a good conductivity. After fabricating four layers photoactive films on ITO electrode, R_{et} value increased to 47 Ω, indicating that the formed compact photoactive multifilms. R_{et} value decreased when the four layers were modified by PEI, due to the positively charged PEI promoted the transfer of the negatively charged redox probe. Thrombin aptamer was covalently immobilized on the electrode surface and then hybridizing with a long complementary DNA, R_{et} had increased to 361 Ω and 443 Ω, respectively. This result turned out that successful assembling thrombin aptamer and the long complementary DNA on the electrode surface. Subsequently, the electrode was interaction with $Ru(NH_3)_6^{3+}$, R_{et} value had decreased sharply to 302 Ω. It was explained that $Ru(NH_3)_6^{3+}$ as a reversible electrochemical active molecule could promote electron-transfer on the electrode surface. After the aptasensor having specific reaction with 4.0 pM thrombin, the diameter of the semicircle became larger than curve f, due to the nonconductive property of large protein.

3.4. Detection of thrombin with PEC aptasensor

After immersing the ITO/(PEI/MPA-G–CdS)$_4$/aptamer–DNA in 0.1 M PBS containing thrombin, the affinity interaction between thrombin aptamer and thrombin brought the thrombin close to ITO surface. This led to the release of long complementary DNA from the multilayer and reduced the amount of the adsorbed $Ru(NH_3)_6^{3+}$, resulting in the decrease of the photocurrent. The decrease of the photocurrent in the presence of thrombin allowed the present system could be used for determination of thrombin. The relationship between the photocurrents and the concentrations of thrombin was displayed in Fig. 4. The photocurrent decrements (ΔI) was defined to the photocurrent differences in the absence and presence of thrombin. The derived calibration curve corresponding of the photocurrent decrements (ΔI) were proportional to the logarithm of thrombin concentrations in a linear range from 2.0 pM to 600.0 pM and the regression equation was ΔI (μA)=2.420+5.813 log($c_{thrombin}$/pM) with a regression coefficient of 0.9845. The sensitivity of ITO/(PEI/MPA-G–CdS)$_4$/aptamer–DNA to thrombin in the presence of $Ru(NH_3)_6^{3+}$ was found to be 0.58 μA/pM. The detection limit was found to be 1.0 pM at 3σ. As a comparison, the photocurrent curves of sensor without further absorption of $Ru(NH_3)_6^{3+}$ showed a linear range from 28.0 pM to 450.0 pM, and the regression equation was ΔI (μA)=0.647 log($c_{thrombin}$/pM)−0.641 with a coefficient of 0.994 (Fig. S-10). The sensitivity of ITO/(PEI/MPA-G–CdS)$_4$/aptamer–DNA to thrombin in the absence of $Ru(NH_3)_6^{3+}$ was found to be 0.065 μA/pM, which was 8.9 times smaller than that of ITO/(PEI/MPA-G–CdS)$_4$/aptamer–DNA in the presence of $Ru(NH_3)_6^{3+}$. The results showed that the developed aptasensor in this study possessed a large linear range and an excellent sensitivity. The aptasensor exhibited the apparent superiority due to the innovation of electron-transfer system and ingenious strategy of dual-signal amplification. The properties and different analytical methods for the detection of thrombin are also summarized and listed in Table 1. As a whole, PEC technique was used for biological assays had more advantages than others. Therefore, this novel superstructure was a promising platform for future development of PEC biosensor.

3.5. Determination of thrombin in serum sample

Sensitive and rapid determination of thrombin in real sample is of great significance for disease diagnosis. To investigate the practicability of the PEC aptasensor, the thrombin was determined in a series of serum samples containing various concentrations of thrombin (Fig. S-11). The serum samples containing thrombin were prepared by adding different amount thrombin into a certain volume of serum. The results was illustrated in Table S-1. The recovery for testing of thrombin in the concentration ranged from 14.0 pM to 450.0 pM was 107.9–94% with relative standard deviation smaller than 5% (1.3–4.6%), showing acceptable detect precision. For detection of thrombin at low concentration of 7 pM, a large deviation for recovery was observed due to low signal-to-noise ratio at low analyte's concentration.

3.6. Stability, specificity and reproducibility of PEC aptasensor

When the as-prepared aptasensor was not in use, it was stored at 4 °C. After two weeks storage, the photocurrent of the

Table 1
Summary of different analytical methods for the detection of thrombin.

Technique	Probe	Amplification	Signal changes	Detection limit (3σ)	Linear range	Ref.
PEC	CdS nanoparticles	Yes	Off	1.0 pM	2.0–600.0 pM	This work
Electrochemical (SWV)	MB	Yes	Off	33 fM	100 fM–1 nM	Zhao et al. (2014)
Electrochemical (ACV)	MB	No	Off	16 nM	–	Cunningham et al. (2014)
Electrochemical (CV)	$[Ru(NH_3)_6]^{3+}$	No	Off	1.0 pM	1 pM–30 nM	Li et al. (2010)
Electrochemical (CV)	$[Fe(CN)_6]^{3-/4-}$	No	Off	0.45 fM	1–100 fM	Wang et al. (2012a)
Electrochemical (DPV)	MB	No	Off	3 nM	6–60 nM	Yan et al. (2011)
ECL	$Ru(NH_3)_6^{2+}$	Yes	Off	45 fM	0.1–200 pM	Yang et al. (2014)
Fluorescence	Silver nanoparticles	No	On	33 pM	0–1000 nM	Cao et al. (2014)
Fluorescence	CdTe QDs	No	On	1.5 μU/mL	10–100 μU/mL	Li et al. (2014b)
Fluorescence	QDs	No	On	10 ng/mL	0.1–1 μg/mL	Tennico et al. (2010)
Fluorescence images	FAM	No	On	0.04 nM	0.04–10 nM	Wang et al. (2012b)
FRET	Carbon nanoparticles	No	On	0.18 nM	0.5–20 nM	Wang et al. (2011)
PEC	Ru(II)–pyrene	No	On	0.1 pM	0–10 pM	Yao et al. (2013)
PEC	CdSe nanoparticles	Yes	On	5.9 fM	20–200 fM	Zhang et al. (2012)
PEC	CdSe nanoparticles	No	Off	0.45 pM	1.0–10 pM	Zhang et al. (2011a)

FRET: fluorescence resonance energy transfer; PEC: photoelectrochemical; ECL: electrochemiluminescent; FAM: 6-carboxyfluorescein; Signal Changes: the change of detection signals along with the thrombin concentration increase is increase (shown on) or is decrease (shown off).

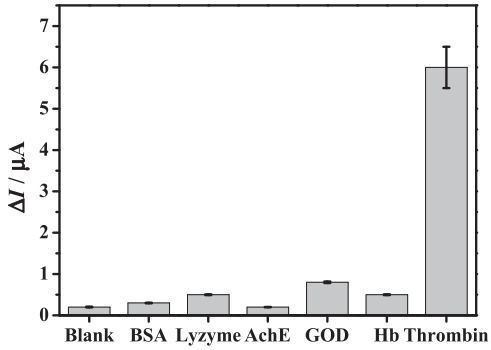

Fig. 5. The specificity of the PEC aptasensor to 4.0 pM thrombin and 10.0 nM other analytes.

aptasensor had not obvious decrease, indicating that the aptasensor had a good stability. The specificity of the aptasensor was tested by replacing of thrombin with other proteins at an excess hundred times concentration of thrombin, including bovine serum albumin, lysozyme, acetylcholine esterase, glucose oxidase and Hb. Nonsignificant change of photocurrent could be observed as for any other proteins comparing with the result obtained in the presence of thrombin only (Fig. 5). This revealed that the proposed aptasensor had an acceptable selectivity due to the specific recognition between aptamer and thrombin. The reproducibility of the aptasensor was also evaluated. The relative standard deviation (RSD) of the photocurrent responses for detection of 4.0 pM thrombin was 4.3% by six different electrodes, suggesting the good reproducibility of this system.

4. Conclusion

In this work, a photoelectrochemical aptasensor was designed for sensitive detection of thrombin. The stable and uniform photoactive multifilms were prepared by alternating adsorption of cationic macromolecules PEI and MPA modified G–CdS nanocomposites. The largest photocurrent signal was observed at an applied potential of +0.2 V and four bilayers of the photoactive multifilms. Thrombin aptamer could be covalently immobilized on the electrode surface by GA cross-linking, which hybridized with a long complementary DNA. After assembling of DNA chain, the photocurrent was increased due to more $Ru(NH_3)_6^{3+}$ absorbed on the electrode surface, which facilitated the electron transfer and promoted the analytical performance of aptasensor. The aptasensor exhibited high sensitivity for thrombin determination with the linear range from 2.0 pM to 600.0 pM and the detection limit of 1.0 pM. Moreover, the aptasensor was approved to have good stability, selectivity and reproducibility. This strategy offered a promising application perspective in the construction of the future PEC biosensors.

Acknowledgments

We gratefully acknowledge the National Basic Research Program of China (Grant 2010CB732400), the Key Program from the National Natural Science Foundation of China (Grant 21035002), the National Natural Science Foundation of China (Grant 21375014 and 21175021), the Social Development Project of Jiangsu (BE2012731) and the Social Development Project of Suzhou (ZXY2012027).

Appendix A. Supplementary information

Supplementary data associated with this article can be found in the online version at http://dx.doi.org/10.1016/j.bios.2014.09.072.

References

An, Y.R., Tang, L.L., Jiang, X.L., Chen, H., Yang, M.C., Jin, L.T., Zhang, S.P., Wang, C.G., Zhang, W., 2010. Chem. Eur. J. 16, 14439–14446.
Bas, D., Boyacı, I.H., 2009. Electroanalysis 21, 1829–1834.
Cao, S.H., Cai, W.P., Liu, Q., Xie, K.X., Weng, Y.H., Huo, S.X., Tian, Z.Q., Li, Y.Q., 2014. J. Am. Chem. Soc. 136, 6802–6805.
Cunningham, J.C., Brenes, N.J., Crooks, R.M., 2014. Anal. Chem. 86, 6166–6170.
Deng, N., Liang, Z., Liang, Yu., Sui, Z.H., Zhang, L.Y., Wu, Q., Yang, K.G., Zhang, L.,.H., Zhang, Y.K., 2013. Biosens. Bioelectron. 42, 556–562.
Gill, R., Patolsky, F., Katz, E., Willner, I., 2005. Angew. Chem. 117, 4630–4633.
Guo, C.Y., Huo, H.H., Han, Xu., Xu, C.L., Li, H.L., 2014. Anal. Chem. 86, 876–883.
Hu, C.G., Zheng, J.N., Su, X.Y., Wang, J., 2013. Anal. Chem. 85, 10612–10619.
Huang, Q.L., Chen, H., Xu, L.L., Lu, D.Q., Tang, L.L., Jin, L.T., Xu, Z.A., Zhang, W., 2013. Biosens. Bioelectron. 45, 292–299.
Ipe, B.I., Lehnig, M., Niemeyer, C.M., 2005. Small 1, 706–709.
Li, H.B., Li, J., Xu, Q., Hu, X.Y., 2011. Anal. Chem. 83, 9681–9686.
Li, L.D., Zhao, H.T., Chen, Z.B., Mu, X.J., Guo, L., 2010. Anal. Bioanal. Chem. 398, 563–570.
Li, J., Li, H.B., Xue, Y., Fang, H.L., Wang., W., 2014a. Sens. Actuators B 191, 619–624.

Li, L.J., Lin, H., Lei, C.Y., Nie, Z., Huang, Y., Yao, S.Z., 2014b. Biosens. Bioelectron. 54, 42–47.
Li, Y.J., Ma, M.J., Zhu, J.J., 2012. Anal. Chem. 84, 10492–10499.
Li, Y.J., Ma, M.J., Yin, G., Kong, Y., Zhu, J.J., 2013. Chem. Eur. J. 19, 4496–4505.
Liang, M.M., Liu, S.L., Wei, M.Y., Guo, L.H., 2006. Anal. Chem. 78, 621–623.
Lin, Y., Zhang, K., Chen, W.F., Liu, Y.D., Geng, Z.G., Zeng, J., Pan, N., Yan, L.F., Wang, X. P., Hou, J.G., 2010. ACS Nano 4, 3033–3038.
Peng, C.Q., Thio, Y.S., Gerhardt, R.A., 2012. Langmuir 28, 84–91.
Qian, Z., Bai, H.J., Wang, G.L., Xu, J.J., Chen, H.Y., 2010. Biosens. Bioelectron. 25, 2045–2050.
Sato, S., Takenaka, S., 2012. Anal. Chem. 84, 1772–1775.
Shen, Q.M., Zhao, X.M., Zhou, S.W., Hou, W.H., Zhu, J.J., 2011. Phys. Chem. C 115, 17958–17964.
Shi, H.J., Zhao, G.H., Liu, M.C., Zhu, Z.L., 2011. Electrochem. Commun. 13, 1404–1407.
Sun, B., Chen, L.J., Xu, Y., Liu, M., Yin, H.S., Ai, S.Y., 2014. Biosens. Bioelectron. 51, 164–169.
Tanne, J., Sch€afer, D., Khalid, W., Parak, W.J., Lisdat, F., 2011. Anal. Chem. 83, 7778–7785.
Tennico, Y.H., Hutanu, D., Koesdjojo, M.T., Bartel, C.M., Remcho, V.T., 2010. Anal. Chem. 82, 5591–5597.
Tian, J.P., Zhao, H.M., Zhao, H.R., Quan, X., 2012. Microchim. Acta. 179, 163–170.
Tu, W.W., Lei, J.P., Wang, P., Ju, H.X., 2011. Chem. Eur. J. 17, 9440–9447.
Wang, G.L., Xu, J.J., Chen, H.Y., Fu, S.Z., 2009a. Biosens. Bioelectron. 25, 791–796.
Wang, G.L., Yu, P.,.P., Xu, J.J., Chen, H.Y., 2009b. J. Phys. Chem. C 113, 11142–11148.
Wang, G.L., Xu, J.J., Chen, H.Y., 2010. Nanoscale 2, 1112–1114.
Wang, L., Zhu, J.B., Han, L., Jin, L.H., Zhu, C.Z., Wang, E.K., Dong, S.J., 2012a. Anal. Chem. 6, 6659–6666.
Wang, Y.H., Bao, L., Liu, Z.H., Pang, D.W., 2011. Anal. Chem. 83, 8130–8137.
Wang, Y.H., Li, M., Zhu, Y.N., Ge, S.G., Yu, J.H., Yan, M., Song, X.R., 2013. Analyst 138, 7112–7118.
Wang, Y.P., Xiao, Y.H., Ma, X.L., Li, N., Yang, X.D., 2012b. Chem. Commun. 48, 738–740.
Xiao, F., Lai, Y.J., Zhang, N.D., Bai, J., Xian, Y.Z., Jin, L.T., 2012. Chin. J. Chem. 30, 1168–1176.
Yan, F.F., Wang, F., Chen, Z.L., 2011. Sens. Actuators B 160, 1380–1385.
Yang, M.L., Chen, Y., Xiang, Y., Yuan, R., Chai, Y.Q., 2014. Chem. Commun. 50, 3211–3213.
Yao, W.J., Alan, L.G., Nicolas, S., Michael, H., Guo, W.D., Dan, S., Eric, D., Serge, C., 2013. Biosens. Bioelectron. 42, 556–562.
Yin, H.S., Sun, B., Zhou, Y.L., Wang, M., Xu, Z.N., Fu, Z.L., Ai, S.Y., 2014. Biosens. Bioelectron. 51, 103–108.
Zeng, X.X., Ma, S.S., Bao, J.C., Tu, W.W., Dai, Z.H., 2013. Anal. Chem. 85, 11720–11724.
Zhang, X.R., Zhao, Y.Q., Li, S.G., Zhang, S.S., 2010. Chem. Commun. 46, 9173–9175.
Zhang, X.R., Li, S.G., Jin, X., Zhang, S.S., 2011a. Chem. Commun. 47, 4929–4931.
Zhang, X.R., Li, S.G., Jin, X., Li, X.M., 2011b. Biosens. Bioelectron. 26, 3674–3678.
Zhang, X.R., Xu, Y.P., Yang, Y.Q., Jin, X., Ye, S.J., Zhang, S.S., Jiang, L.L., 2012. Chem. Eur. J. 18, 16411–16418.
Zhao, J., Hu, S.S., Zhong, W.D., Wu, J.G., Shen, Z.M., Chen, Z., Li, G.X., 2014. Appl. Mater. Interfaces 6, 7070–7075.
Zhao, W.W., Ma, Z.Y., Yan, D.Y., Xu, J.J., Chen, H.Y., 2012a. Anal. Chem. 84, 10518–10521.
Zhao, W.W., Ma, Z.Y., Yu, P.P., Dong, X.Y., Xu, J.J., Chen, H.Y., 2012b. Anal. Chem. 84, 917–923.
Zhao, W.W., Yu, P.P., Shan, Y., Wang, J., Xu, J.J, Chen, H.Y., 2012c. Anal. Chem. 84, 5892–5897.
Zhao, W.W., Shan, S., Ma, Z.Y., Wan, L.N., Xu, J.J., Chen, H.Y., 2013. Anal. Chem. 85, 11686–11690.
Zhao, X.M., Zhou, S.W., Jiang, L.P., Hou, W.H., Shen, Q.M., Zhu, J.J., 2012d. Chem. Eur. J. 18, 4974–4981.